Published in final edited form as:
Eur J Neurosci. 2010 November ; 32(9): 1461–1472. doi:10.1111/j.1460-9568.2010.07431.x.

LACK OF PROTEIN-TYROSINE SULFATION DISRUPTS PHOTORECEPTOR OUTER SEGMENT MORPHOGENESIS, RETINAL FUNCTION AND RETINAL ANATOMY

David M. Sherry[1,2], **Anne R. Murray**[1], **Yogita Kanan**[1], **Kelsey L. Arbogast**[1], **Robert A. Hamilton**[1], **Steven J. Fliesler**[3], **Marie E. Burns**[4], **Kevin L. Moore**[1,5], and **Muayyad R. Al-Ubaidi**[1,2]

[1]Department of Cell Biology, University of Oklahoma Health Sciences Center, Oklahoma City, OK

[2]Oklahoma Center for Neurosciences, University of Oklahoma Health Sciences Center, Oklahoma City, OK

[3]Research Service, VA Western New York Healthcare System, and Departments of Ophthalmology and Biochemistry, University of Buffalo/State University of New York, Buffalo, NY

[4]Center for Neuroscience and Department of Ophthalmology and Vision Science, University of California, Davis, CA

[5]Cardiovascular Biology Research Program, Oklahoma Medical Research Foundation, and the Departments of Cell Biology and Medicine, University of Oklahoma Health Sciences Center, Oklahoma City, Oklahoma

Abstract

To investigate the role(s) of protein-tyrosine sulfation in the retina, we examined retinal function and structure in mice lacking tyrosylprotein sulfotransferases (TPST) 1 and 2. *Tpst* double knockout (DKO; *Tpst1*$^{-/-}$/*Tpst2*$^{-/-}$) retinas had drastically reduced electroretinographic responses, although their photoreceptors exhibited normal responses in single cell recordings. These retinas appeared normal histologically; however, the rod photoreceptors had ultrastructurally abnormal outer segments, with membrane evulsions into the extracellular space, irregular disc membrane spacing, and expanded intradiscal space. Photoreceptor synaptic terminals were disorganized in *Tpst* DKO retinas, but established ultrastructurally normal synapses, as did bipolar and amacrine cells; however, the morphology and organization of neuronal processes in the inner retina were abnormal. These results indicate that protein-tyrosine sulfation is essential for proper outer segment morphogenesis and synaptic function, but is not critical for overall retinal structure or synapse formation, and may serve broader functions in neuronal development and maintenance.

Keywords

mouse; retina; extracellular matrix; tyrosine *O*-sulfation; retinal degeneration

*To whom correspondence should be addressed: Department of Cell Biology, University of Oklahoma Health Sciences Center, BMSB 781, 940 Stanton L. Young Blvd., Oklahoma City, OK 73104, Voice (405) 271-2382, Fax (405) 271-3548, muayyad-al-ubaidi@ouhsc.edu.
Section editor: Dr. Timothy J. Collier
Associate Editor: Dr. Christian Grimm

INTRODUCTION

Protein-tyrosine sulfation, first documented on fibrinogen by Bettelheim in 1954 (Bettelheim 1954), is one of the many post-translational modifications that occur in eukaryotic cells. Although tyrosine sulfation is a common post-translational modification (Huttner 1982;Moore 2003;Moore 2009), the functions of tyrosine sulfation *in vivo* are only now being explored.

The enzymes responsible for tyrosine sulfation, the tyrosyl:protein sulfotransferases (TPSTs), are membrane-bound and localize to the *trans*-Golgi compartment of the cell, where they transfer the sulfuryl group from 3'-phosphoadenosine 5'-phosphosulfate onto tyrosine residues in polypeptides (Lee and Huttner 1983). Two TPST enzymes, designated TPST-1 and TPST-2, have been identified in humans and mice (Moore 2003) and their corresponding genes have been cloned and characterized (Ouyang et al 1998;Ouyang and Moore 1998).

Recent studies using *Tpst1* and *Tpst2* knockout mice have begun to provide new insights into the biological importance of tyrosine sulfation. TPST-1 knockout ($Tpst1^{-/-}$) mice have approximately 5% lower average body weight than their wild-type (*wt*) controls and $Tpst1^{-/-}$ females produce smaller litters, on average, than *wt* females as a consequence of increased embryonic death between 8.5 and 15.5 days postcoitum (Ouyang et al 2002). TPST-2 knockout ($Tpst2^{-/-}$) mice exhibit moderately delayed growth, although they appear healthy and reach normal body weight by 10 weeks of age. $Tpst2^{-/-}$ males are infertile, despite their sperm being indistinguishable from *wt* males in regards to morphology, number, motility in normal media, and ability to capacitate and undergo acrosomal exocytosis (Borghei et al 2006). More recent studies have demonstrated that the *grt* mouse, a spontaneous mouse mutant with an inactivating mutation in the *Tpst2* gene, and $Tpst2^{-/-}$ mice have primary hypothyroidism likely due to hyporesponsiveness of the thyroid-stimulating hormone receptor (Sasaki et al 2007;Westmuckett et al 2008). While both $Tpst1^{-/-}$ and $Tpst2^{-/-}$ mice have normal life spans, $Tpst1^{-/-}/Tpst2^{-/-}$ double knockout (*Tpst* DKO) mice have a very high post-natal mortality rate and rarely survive beyond weaning age (Westmuckett et al 2008). Despite the evidence that suggests tyrosine sulfation has important biological functions, the functional significance of tyrosine sulfation in the central nervous system has not been explored.

Tyrosine-sulfated proteins are present in the retina of species from fish to humans and both *Tpst1* and *2* transcripts are expressed in the retina (Kanan et al 2009), making available an excellent model system to study the functional roles of tyrosine sulfation in the central nervous system. We utilized wildtype and *Tpst* DKO mice to investigate the role of tyrosine sulfation in the establishment and maintenance of retinal structure and function. Retinas of *Tpst* DKO mice showed dramatic reduction in overall function despite the fact that the individual rod photoreceptors were functionally competent. Retinas of *Tpst* DKO mice appeared normal when examined at the light microscopic level. However, ultrastructural analysis found that *Tpst* DKO retinas exhibited severe malformations of rod photoreceptor outer segment (OS). Additionally, photoreceptor terminals in the *Tpst* DKO retina appeared disorganized, although they were able to establish ultrastructurally normal ribbon synapses. Immunohistochemistry (IHC) revealed that disrupted tyrosine sulfation produced cell-specific deficits in the morphology and organization of neuronal processes in the inner retina. These findings suggest that tyrosine sulfation may have broader, unrecognized roles in neuronal morphogenesis and establishment of connections within the central nervous system.

MATERIALS AND METHODS

Animals

Tpst1 null (Tpst1^{tm1Klm}, MGI:2183366) and *Tpst2* null (Tpst2^{tm1Klm}, MGI:3512111) and *Tpst* DKO mice were generated, characterized, housed, and fed as previously described (Borghei et al 2006;Ouyang et al 2002;Westmuckett et al 2008). Supporting previous findings, *Tpst* DKO animals (both sexes) had poor postnatal survival and only rarely survived beyond weaning (Westmuckett et al 2008).

All experiments involving animals were approved by the local Institutional Animal Care and Use Committees and conformed to the *National Institute of Health Guide for the Care and Use of Laboratory Animals* and the *Association for Research in Vision and Ophthalmology Resolution on the Use of Animals in Research*.

Electroretinography

Electroretinograms (ERGs) were recorded from the corneal surface of mice as described by (Xu et al 2000). Briefly, rod photoreceptor function was assessed by presenting a 140 candela (cd)-s/m^2 flash stimulus to the dark-adapted, dilated mouse eyes in a LKC UTAS-E3000 Ganzfeld (LKC Technologies, Inc., Gaithersburg, MD). To evaluate the light response of cones, a strobe 79 cd-s/m^2 flash stimulus was presented to light-adapted (5 min, **29 cd/m^2**), dilated eyes in the same apparatus. Responses were recorded and then analyzed using EM for Windows (LKC Technologies, Inc.).

Light and Electron Microscopy

Methods used for tissue collection, processing for Spurr's resin-embedment, microtomy and subsequent examination by light (LM) and electron microscopy (EM) were as previously described (Stricker et al 2005). For LM, 0.75–1μm thick tissue sections were examined and photographed with an Olympus BH-2 photomicroscope (auto-expose mode) using 20× or 60× DPlanApo objectives, and images were obtained and stored on a PC computer using a Nikon DXM-1200 digital camera system. For EM, silver-gold tissue sections were viewed with a JEOL 100 EX electron microscope (accelerating voltage, 80 KeV).

To assess the integrity of the OPL, electron micrographic images taken at a magnification of 5000× were evaluated for the following well-known ultrastructural features of the OPL (*e.g.*, (Dowling 1968)): placement, size, and spacing of rod and cone terminals and the location of processes from second-order neurons within the layer. To assess the integrity of photoreceptor synapses, electron microscopic images of rod and cone photoreceptor terminals taken at a magnification of 26,000–33,000× were examined for the following features: the presence of synaptic ribbons with associated vesicles, the presence of an attachment anchoring the ribbon to the plasma membrane of the terminal, the presence of post-synaptic processes apposed to the ribbon and their arrangement in the typical triad conformation of lateral processes flanking the ribbon and a central process located immediately under the ribbon. In the case of cones, the presence of flat contacts along the base of the terminal also was examined.

Immunohistochemistry and lectin cytochemistry

Most immunohistochemistry (IHC) and lectin cytochemistry analyses were performed on frozen sections of eyes from *wt* and *Tpst* DKO mice, although some lectin labeling studies were performed on sections of paraffin-embedded eyes. For IHC, following euthanasia of the animal, the eyes were quickly enucleated, the cornea was punctured, and the eyes were immersed in cold 4% (w/v) paraformaldehyde in 0.1 M cacodylate buffer (pH 7.2) for 30 min to 2 h. The anterior portion of the eye was trimmed away; the resulting eyecup was

rinsed in phosphate-buffered saline (pH 7.2), then serially cryoprotected using 15% and then 30% (w/v) sucrose in PBS. Eyes were frozen in OCT mounting medium and sectioned on a cryostat at a thickness of 10–15 μm. Sections were mounted on slides and stored at −20°C until ready for use.

Immunolabeling was performed as described previously (Sherry et al 2006). In brief, sections were rehydrated, pre-treated with 1% $NaBH_4$ to reduce autofluorescence, rinsed, and then blocked (10% normal goat serum, 5% BSA, 1% fish gelatin, and 0.5% Triton X-100 in Hank's buffered saline solution) to reduce non-specific labeling. Excess blocking solution was removed, and primary antibodies diluted in blocking solution were applied for 16–48 h. For double- and triple labeling, primary antibodies were applied simultaneously. Sections were rinsed, blocked again, and incubated in an appropriate combination of secondary antibodies conjugated to AlexaFluor dyes (Invitrogen-Molecular Probes, Carlsbad, CA; diluted 1:200–1:500) for 1–1.5 h. Sections were rinsed and mounted in ProLong Gold Antifade Reagent (Invitrogen-Molecular Probes, Carlsbad, CA) to retard bleaching. Details of the antibodies used for immunolabeling studies are provided in Supplemental Table 1. All antibodies were diluted in blocking solution. Specificity of immunolabeling was tested by omitting monoclonal primary antibodies or by substituting normal serum from the same host for polyclonal primary antibodies, and then processing as described above and treating with a combination of secondary antibodies. Immunolabeling appeared in only those specimens treated with primary antibody, as appropriate.

For lectin labeling, 5-μm thick sections of paraffin-embedded eyes from *wt* and *Tpst* DKO mice were prepared. Sections were deparaffinized, rehydrated and treated with 1% $NaBH_4$ to reduce autofluorescence, rinsed, and incubated for 1–1.5 h at room temperature in a mixture of WGA and PNA conjugated to AlexaFluor488 or AlexaFluor568, respectively (Diluted 1:10–1:20 in the blocking solution as described above for antibody staining). Sections were rinsed, coverslipped using ProLong Gold® Antifade Reagent, as above.

Labeling was visualized using an Olympus BX61WI fluorescence microscope (Olympus America, Center Valley, PA) equipped with a Hamamatsu ORCA-ER camera (Hamamatsu, Bridgewater, NJ). Image acquisition was controlled through Slidebook® software (Intelligent Imaging Innovations, Denver, CO). To prepare figures, images were exported to Photoshop (Adobe, Mountain View, CA) and brightness, contrast and threshold were adjusted to highlight specific labeling.

Immunoblot (Western) analysis

Western blots were processed as described before (Tan et al 2001) and images were obtained using a Kodak image station (Carestream Molecular Imaging, Rochester, NY).

Relative Quantitative RT-PCR

Quantitative RT-PCR (qRT-PCR) was performed as previously described (Farjo et al 2006). Retinas were obtained and extracted from 3–5 animals (age and genotype indicated on figure) using TRIzol® reagent (Invitrogen, Carlsbad, CA, U.S.A.). Equivalent amounts of RNA were used for the synthesis of cDNA using an oligo-dT primer and SuperScript III RT in the SuperScript™ III First-Strand Synthesis System for RT-PCR (Invitrogen, Carlsbad, California, U.S.A.). The generated cDNA was diluted 10-fold and the dilutions were used in subsequent qRT-PCR reactions. Primers were designed to span introns to avoid amplification from genomic DNA. Also, the primers for *Tpst1* and *Tpst2* were designed to include the portion of the gene that was replaced with a Neo cassette in the generation of the $Tpst1^{-/-}$ and $Tpst2^{-/-}$ mice (Borghei et al 2006;Ouyang et al 2002). Two independent qRT-PCR experiments were performed. Each one was performed in triplicate on 3–5 individual

cDNA samples using the iCycler machine (Bio-Rad, Hercules, CA), and ΔcT values were calculated against the neuronal housekeeping gene *Hprt*. *Hprt* was assigned an arbitrary expression level of 1,000, and relative gene expression values were calculated as follows: relative expression = $1{,}000/2^{\Delta cT}$, where ΔcT = (gene cT – *Hprt* cT). Disassociation curve analysis and gel electrophoresis were performed on all PCR products to confirm proper amplification.

Gene	Forward primer sequence (5' → 3')	Reverse primer sequence (5' → 3')	Amplicon size	Efficiency
HPRT	GCAAACTTTGCTTTCCCTGGTT	CAAGGGCATATCCAACAACA	152	109
Tpst1	TATCGAAGTGGGTTGGGAAG	GTCGTCCCTGTGGGAAGTTA	233	112
Tpst2	ACACAGTCCTGCACCATGAG	ATTCGCATACGGGTCATAGC	206	94

Suction electrode recording

Suction electrode recording from intact mouse rods was performed as previously described (Krispel et al 2003). Briefly, a mouse was dark-adapted overnight and on the day of the experiment the eyes were removed under infrared light following anesthesia and decapitation. Using a microscope equipped with IR/Vis spectrum converters, the retinas were dissected into chilled oxygenated L-15 media, and stored on ice in a lightproof box. For each recording, a piece of retina was chopped into small pieces and placed in a chamber perfused with oxygenated Locke's salt solution warmed to 37°C. Under IR light that did not activate rhodopsin (RHO), a rod photoreceptor was selected and drawn into the suction electrode containing HEPES-buffered Locke's solution connected via an agar bridge to one half-cell of a calomel electrode. The reference half-cell was connected via an agar bridge to the bath. The output was amplified by a current-to-voltage converter (Axopatch 200; Axon Instruments), low-pass filtered by an 8-pole Bessel filter with a 30 Hz corner frequency, and digitized via a National Instruments MIO board in IgorPro 4.0 (Wavemetrics; Lake Oswego, OR). Data were analyzed off-line using custom-written macros in Igor Pro.

Light (500 nm; 10 nm FWHM; 10 ms duration) intensities were controlled by calibrated neutral density filters, and the power of the lamp was measured after each day through the relevant interference filters by placing a silicon photodiode (UDT350, UDT Instruments, Orlando, FL) at the location of the recording chamber.

Statistical Analysis

Unless otherwise stated, statistical significance was determined using ANOVA with Bonferroni *post hoc* multiple pairwise comparison tests (PRISM™; GraphPad® Software, San Diego, CA). For suction electrode recordings, statistical significance was determined using a two-tailed Student's *t*-test, assuming equal variances.

RESULTS

Postnatal pattern of expression of TPSTs

We have shown that the retina expresses several sulfated proteins as well as the transcripts for both *Tpst1* and *−2* (Kanan et al 2009). To determine the developmental onset of expression of both enzymes and to quantify the relative (to *Hprt*) levels of their transcripts, quantitative real-time PCR (qRT-PCR) analysis was performed. Both *Tpst1* and *Tpst2* are expressed on postnatal day (P) 1, the earliest time point tested (Figure 1). Transcript levels for both enzymes fluctuated over the course of retinal development. Both transcripts had

their highest expression levels during early postnatal development and decreased by P30. Both enzymes had second peaks of elevated transcript expression on P60 with subsequent gradual declines to low levels by P300.

Levels of transcripts for both enzymes were also determined in retinas of P30 *Tpst1*$^{-/-}$ and *Tpst2*$^{-/-}$ mice (Figure 1). The *Tpst2*−/− retina expressed somewhat higher levels (≥ 2-fold) of *Tpst1* than the *wt* retina (Figure 1A), suggesting some level of compensation for the lack of TPST-2 may exist. However, the converse was not true: *Tpst2* transcript levels in the *Tpst1*$^{-/-}$ retina at P30 were indistinguishable from those in *wt* retina at P30.

Previous Western blot analysis using the anti-sulfotyrosine antibody PSG2 found that the retina contains several tyrosine-sulfated proteins, some of which are cell type specific (Kanan et al 2009). IHC using the PSG2 antibody localized tyrosine-sulfated proteins to all retinal layers as well as to the retinal pigmented epithelium (RPE) and sclera (Figure 1C), as previously shown (Kanan et al 2009). Protein-tyrosine sulfation was not found in the retina, RPE and sclera of *Tpst* DKO mice as indicated by the absence of labeling (Figure 1C).

Retinal function and structure in Tpst DKO mice

To determine how the complete loss of retinal protein-tyrosine sulfation affects retinal function, *Tpst* DKO animals were examined by ERG. Compared to age-matched *wt* littermates, weanling (P21) *Tpst* DKO mice show severe scotopic (~25% of normal *a*-wave) and photopic (~15% of normal) ERG response deficits (Figure 2 and Supplemental Figure 1). Part of the reduction (~42%) in the scotopic *b*-wave can be accounted for by the reduction in scotopic *a*-wave (Figure 2A&B). This suggests a role for tyrosine sulfation in photoreceptors and second-order retinal neurons. However, the reduction in the photopic responses is more severe than that in the scotopic responses, which suggests a more important role for tyrosine sulfation in the development of cone function. Despite the dramatic reductions in the ERG responses in *Tpst* DKO mice, their retinas were histologically comparable to the retinas of age-matched *wt* littermates (Figure 2D–E). Hence, the absence of protein-tyrosine sulfation disrupted retinal function without causing gross disruption of retinal structure. Because of the poor postnatal survival of *Tpst* DKO mice, it was not possible to assess whether retinal function improved with age.

Suction electrode recordings from Tpst DKO rod photoreceptors

Because some tyrosine-sulfated proteins are known to be secreted, while others are retained on the cell surface (Hille et al 1990;Hille and Huttner 1990;Kanan et al 2009), the deficits observed in the ERG responses might have arisen from intrinsic defects in the photoreceptors themselves or from extrinsically induced changes due to the absence of tyrosine sulfation on secreted proteins. Therefore, suction electrode recordings of rods from P22 *Tpst* DKO and *wt* mice were performed to determine whether the intrinsic flash responses of rods from *Tpst* DKO retinas were altered.

The retinas of P22 *Tpst* DKO mice were normal in appearance and readily yielded rods with straight OS that could be easily drawn into the recording electrode. In contrast to the profound ERG deficits described above, *Tpst* DKO rods generated flash responses that were nearly normal (Figure 2F&G). *Tpst* DKO rods had maximal response amplitudes that were slightly smaller than normal (p=0.003; “Dark current” in Table 1), though current up to 20 pA was recorded in one example (Figure 2F&G). This decrease in average dark current may have resulted from smaller functional OS, as other measures that strongly depend on OS functional volume were also affected. For example, the size of the OS can affect the number of photons that are absorbed from a given flash (Baylor et al 1979); indeed, *Tpst* DKO rods displayed slightly smaller effective collecting areas (p=0.21; in μm^2: *Tpst* DKO, 0.30 ± 0.08

(n=7); *wt*, 0.41 ± 0.04 (n=27)) and decreased sensitivity (I_o; Table 1, p=0.01). *Tpst* DKO rod responses to bright flashes also recovered slightly more rapidly than those of *wt* rods (Table 1, τ_D; p=0.00003). None of the characteristics of the dim flash response were affected (p > 0.2; Table 1), including time to peak, elementary amplitude (single photon response), integration time, or time constant of recovery for dim flashes (τ_{rec}). These data clearly indicate that the lack of tyrosine sulfation did not affect the rods' ability to generate and maintain a standing dark current, nor to activate and deactivate the phototransduction cascade. These results also suggest that the ERG deficits observed in the *Tpst* DKO mice may arise (among other possibilities) from defects extrinsic to the retinal cells themselves, possibly tyrosine-sulfated proteins associated with the interphotoreceptor matrix (IPM) (Kanan *et al*., 2009).

Tyrosine sulfation is essential for normal rod and cone outer segment structure

The OS of photoreceptors comprise a stack of membranous disks that house the light-sensitive visual pigments and other components needed for visual transduction. The morphogenesis and structure of the OS are intimately related to the IPM, which contains tyrosine-sulfated proteins (Kanan et al 2009). To assess whether the lack of tyrosine sulfation disrupted OS morphogenesis, we examined OS ultrastructure. In the normal rod OS, the membranous disks are tightly stacked, discontinuous with the surrounding plasma membrane, and completely separated from the extracellular space (Figure 3A&C). However, in the *Tpst* DKO retina, rod OS structure is severely disrupted (Figure 3B&D), with irregular interdiscal spacing and enlarged intradiscal spaces. In addition, rod OS in the *Tpst* DKO retina had numerous abnormal membranous extensions into the extracellular space that often appeared to arise from protruding discs. The possibility that the plasma membrane also contribute to these aberrant membrane protrusions could not be ruled out.

The normal cone OS is comprised of a stack of tightly packed membranous lamellae that are continuous with the plasma membrane and in direct contact with the extracellular space (Figure 3E&G). In contrast to the severe disruption of rod OS ultrastructure, the structure of the cone OS in the *Tpst* DKO retina showed little disruption (Figure 3F&H). Cone OS discs were well organized and showed normal rim structure, although some increase in the intradiscal space was observed in some discs (Figure 3G&H). This finding suggests that unlike the case in rod photoreceptors, where OS disruption may contribute to the decline in the *a*-wave, the reduced photopic ERG responses in *Tpst* DKO mice cannot be attributed to OS changes in cones.

To determine whether the reduced photopic ERG resulted from reduced number of cones in the *Tpst* DKO retina, immunoblot analysis of cone opsins was performed. When compared to actin, the levels of M- and S-cone opsins in the *Tpst* DKO were similar to those in the *wt* retinas (Supplemental Figure 2A).

The IPM surrounding rod and cones OS can be selectively visualized using suitably labeled wheat germ agglutinin (WGA) and peanut agglutinin (PNA), respectively (Blanks and Johnson 1983;Blanks and Johnson 1984;Sameshima et al 1987). To determine whether lack of sulfation disrupts the IPM, both WGA and PNA were visualized on retinal sections from *wt* and *Tpst* DKO retinas. Labeling for WGA and PNA revealed that the rod- and cone-specific domains of the IPM were still present in the *Tpst* DKO retina (Figure 4). Qualitative examination of the sections in Figure 4 (C&D) suggests that the number of cones in the *Tpst* DKO retina is very similar to that observed in *wt* retinas, a result in agreement with the findings from the immunoblot analysis presented in Supplemental Figure 2A. However, the IPM sheaths around the OS were shorter in the *Tpst* DKO retina than in the *wt* retina. These data are consistent with the disrupted OS ultrastructure observed in the absence of tyrosine sulfation.

Together, these results indicate that tyrosine sulfation is essential for proper morphogenesis and maintenance of rod OS structure, and that the rod OS anomalies observed in the *Tpst* DKO retinas may contribute to aberrant rod function *in situ* and the smaller ERG *a*-waves obtained from *Tpst* DKO animals. In contrast, cone OS in the *Tpst* DKO retina showed comparatively little ultrastructural disruption.

The absence of tyrosine sulfation produces minor effects on the structural organization and synapses in the inner retina

To determine whether tyrosine sulfation affected the neurons or the structural and synaptic organization of the inner retina, we examined the organization of the various types of retinal cells and their processes using a panel of well-characterized cell- and synapse-specific markers (Supplemental Table 1).

To test whether the lack of tyrosine sulfation might specifically disrupt bipolar cells, we examined expression of proteins related to reception of glutamatergic signals from photoreceptors, and to bipolar cell structure and synaptic terminals. $G_{\alpha}o$ and Gγ13 are heterotrimeric G-protein subunits needed for glutamatergic transmission from photoreceptors to ON type bipolar cells (the rod and ON-cone bipolar cells). Immunolabeling for $G_{\alpha}o$ and Gγ13 showed that ON type bipolar cells in the *Tpst* DKO retina continued to express these key proteins, although labeling intensity was somewhat reduced (Figure 5), suggesting that ON type bipolar cells still expressed the transduction machinery needed for transmission from photoreceptors. Labeling for the transcription factors Islet-1 and Chx-10, which together identify and distinguish the ON and OFF bipolar cell populations (Burmeister et al 1996;Elshatory et al 2007), revealed that both ON and OFF bipolar cell types were present and migrated to their proper position in the inner nuclear layer (INL) in the *Tpst DKO* retina (Supplemental Figure 3). Labeling using markers for specific populations of bipolar cells and their synaptic terminals showed that cell-specific bipolar cell morphology and synaptic projections to the IPL were unaffected in the *Tpst* DKO retinas (Figure 6; PKC, synaptotagmin 2, and VGLUT1 shown), although the Type 6 ON-cone bipolar cell plexus in the IPL was enlarged (Figure 6G). Furthermore, bipolar cell terminals in the *Tpst* DKO retina expressed appropriate cell-specific synaptic proteins (*i.e*., VGLUT1, Figure 6; Supplemental Table 2).

Similarly, immunolabeling for cell specific markers for several subtypes of amacrine cells, horizontal cells, ganglion cells, and Müller glial cells showed that all of these cell populations were present in the *Tpst* DKO retina and morphologically normal, although the plexes of some amacrine cell types in the IPL were somewhat reduced (Supplemental Figures 4 and 5; Supplemental Table 2). Expression of cell-specific synaptic proteins was also unaffected, although immunolabeling levels were somewhat reduced in some cases (Supplemental Table 2).

Although the absence of tyrosine sulfation did result in somewhat reduced immunolabeling for some proteins and subtle morphological changes in specific types of retinal cells, such as the increased size of Type 6 ON-cone bipolar cell plexus in the IPL, western blot analysis indicated that protein expression levels did not change substantially between *wt* and *Tpst* DKO retina (*e.g*., synaptotagmin 2, Supplemental Figure 2B). Together, these results indicated that the absence of tyrosine sulfation did not induce large scale alterations in retinal cell populations, their differentiation, or their structural organization.

To test whether the absence of tyrosine sulfation disrupted retinal function by disrupting synapse formation or structure, we also examined synapses in the OPL and IPL by electron microscopy. The OPL of the *Tpst* DKO retina showed greater spacing between photoreceptor terminals and greater variability in terminal shape than in the *wt* retina (Figure

7A–B). Individual rod and cone terminals in the *wt* and *Tpst* DKO retina formed normal ribbon synaptic complexes characterized by a triad of post-synaptic processes from horizontal and bipolar cells associated with a synaptic ribbon anchored to the plasma membrane of the photoreceptor terminal (Figure 7C–F). Cone terminals in both *wt* and *Tpst* DKO retinas also formed normal flat contacts with bipolar cell processes (Figure 7E–F). Although ultrastructurally normal rod and cone synapses were present in the *Tpst* DKO retina, rod and cone terminals that showed ultrastructural aberrations also were observed (Figure 7G, H). Abnormalities included malformed presynaptic ribbons (Figure 7G, rod terminal shown), abnormal interactions with processes from second-order neurons (Figure 7H, cone terminal shown), and synaptic ribbons that were not anchored to the plasma membrane (see cone terminal in Figure 7B).

In the IPL, bipolar and amacrine cells in the *Tpst* DKO retina formed synapses with ultrastructure and organization similar to the bipolar and amacrine cell synapses of the *wt* retina. Bipolar cell synapses in both *wt* and *Tpst* DKO retinas displayed the normal “dyad” synaptic ultrastructure with postsynaptic processes of amacrine and ganglion cells apposed pair-wise to small presynaptic ribbons in the bipolar cell terminal (Figure 8A–B). Amacrine cells in the *Tpst* DKO retina formed ultrastructurally normal conventional synapses in the IPL comparable to those seen in the IPL of the *wt* retina (Figure 8C–D).

DISCUSSION

To investigate the role(s) of protein-tyrosine sulfation in retinal function and structure, mice lacking both TPST-1 and -2 were examined. ERG *a*-wave responses from *Tpst* DKO retina were severely reduced, indicating that photoreceptor function was compromised in the absence of protein-tyrosine sulfation. Despite aberrant OS ultrastructure and reduced ERG *a*-wave responses, suction electrode recordings of rods lacking both *Tpst1* and *Tpst2* exhibited light flash responses very similar to those from *wt* rods, indicating that the *a*-wave ERG changes resulted from deficits extrinsic to the rod phototransduction machinery itself. Additionally, ERG *b*-wave amplitudes were substantially smaller in *Tpst* DKO mice than in *wt* mice, although the photoreceptor terminals in the OPL of the *Tpst* DKO retina established ribbon synapses and bipolar cell dendrites showed no obvious structural deficits. These findings suggest that the absence of tyrosine sulfation impaired transmission from photoreceptors to bipolar cells without producing large-scale disruptions in OPL structure.

The functional and structural phenotypes in the OS of the *Tpst* DKO retina could arise as a direct consequence of the lack of sulfation of retinal proteins. Alternatively, it could result from reduced amount of RHO in the OS, impacting both the functional and structural characteristics of the retina. However, this is unlikely since immunoblot analysis showed no changes in RHO amounts in *Tpst* DKO retinas (data not shown). Furthermore, reduction of RHO levels by 50% in the $rho^{+/-}$ retina (Lem et al 1999) does not result in ERG changes similar to those reported here. The phenotype observed in *Tpst* DKO retinas could arise indirectly from hypothyroidism, since primary hypothyroidism is a feature of the *grt*/*grt* mouse, which is characterized by lack of sulfation by TPST-2 and fetal-onset severe thyroid hypoplasia (Sasaki et al 2007). Chemically induced congenital and neonatal hypothyroidism significantly reduces thickness, layering, volume, cell number and nuclear volumes in the retinas of Wistar rats (Pinazo-Duran et al 2005). However, comparable alterations were not observed in the retina of *Tpst* DKO mice, suggesting that *Tpst* DKO mice receive sufficient maternally-derived thyroid hormone during development to support proper retinal histogenesis. Therefore, the functional and ultrastructural alterations observed in the *Tpst* DKO retina arise from the lack of tyrosine sulfation of retinal proteins, rather than a lack of thyroid hormone.

A major finding of this study is that the absence of tyrosine sulfation severely compromised the normal ultrastructural organization of the rod OS: the dense, regular packing of discs within the rod OS was disrupted, the intradiscal spacing was enlarged, and discs extended aberrantly into the extracellular space between adjacent rod OSs. Despite the severity of the ultrastructural defects in the OS, individual rods in the *Tpst* DKO retina were still able to generate essentially normal light responses when removed from the eye, as shown by suction electrode recordings. In contrast, cone OSs maintained largely normal ultrastructure. Because *Tpst* DKO mice had dramatically smaller ERG *a*-wave amplitudes, these results suggest that photoreceptor function *in vivo* may be strongly influenced by the extracellular milieu. The IPM, which is important for OS morphogenesis and maintenance and is known to contain tyrosine-sulfated proteins (Kanan et al., 2009), is a leading candidate to contribute to disrupted rod OS ultrastructure in the *Tpst* DKO retina. However, the absence of tyrosine sulfation did not eliminate formation of the rod- or cone-specific IPM nor disrupt its organization at a gross level as demonstrated by lectin cytochemistry. Therefore, the disrupted rod OS ultrastructure in the *Tpst* DKO retina is likely to result from disruption of specific molecular interactions between the IPM and the OS or between components within the IPM, rather than a failure to secrete the IPM or to form rod- and cone-specific domains within the IPM.

Absence of large scale disruption of retinal structure, cell populations, or organization of retinal neurons in the Tpst DKO retina

Although the absence of tyrosine sulfation affected retinal function, effects on retinal structure were limited. An important finding is that all of the retinal cell types and subpopulations examined were present in the *Tpst* DKO retina and showed appropriate cell-specific placement, morphology, and organizational characteristics as well as the ability to form synapses. The anatomical and ultrastructural findings taken together with the reduced ERG a-wave in the *Tpst* DKO retina strongly support the notion that the observed deficits in retinal function arise mainly at the level of the photoreceptors rather than the inner retina. The absence of tyrosine sulfation resulted in a generalized reduction in the extent of the neuronal plexes in the synaptic layers, consistent with the expression of *Tpst-1* and/or *-2* by all cells. However, it is important to note that the lack of tyrosine sulfation did not disrupt the laminar organization of bipolar and amacrine cell processes in the IPL, which is a critical cell-specific attribute that determines the synaptic and functional organization of inner retinal circuits. The plexes of amacrine cells appeared somewhat more sensitive to tyrosine sulfation deficiency than the plexes of other cell types, with the plexes of VGLUT3 and starburst amacrine cells being most sensitive. An interesting exception is the Type 6 ON-cone bipolar cell, which normally forms a sparse plexus in the ON sublamina of the IPL (Fox and Sanes 2007;Wassle et al 2009), but formed an expanded plexus in the IPL of the *Tpst* DKO retina. These findings suggests that tyrosine sulfated proteins can affect the development, organization and/or maintenance of neurites in a cell-specific manner.

Synaptic contacts are formed in absence of tyrosine sulfation

Our ultrastructural studies show that tyrosine sulfation is not essential for synapse formation, as normal synapses were made by all types of retinal neurons in the *Tpst* DKO retina. However, the presence of ultrastructurally abnormal ribbon synaptic complexes in the photoreceptor terminals of the *Tpst* DKO retina, suggests that tyrosine sulfation deficiency can affect synapse formation, maintenance and/or function and could contribute to reduced transmission from photoreceptors to bipolar cells as indicated by the reduced b-wave of the *Tpst* DKO retina. In contrast, the synapses in the IPL showed normal ultrastructural characteristics. However, it should be noted that normal synaptic ultrastructure does not necessarily indicate normal synaptic function. As discussed above, synaptic proteins were expressed in an appropriate synapse-specific manner in the *Tpst* DKO retina, although the

levels of some of these proteins may have been reduced in some synapses, which potentially could affect synaptic function.

It should be noted that the current study does not address whether the lack of tyrosine sulfation affects the total numbers of synapses formed or large-scale patterns of connectivity between neurons in retinal circuits, which could affect retinal function without causing neurochemical or structural changes that can be detected easily with the methods utilized.

The mechanisms by which tyrosine sulfation might affect development and/or maintenance of synaptic connections or functional transmission are not known. Because tyrosine sulfation is a common post-translational modification of secreted proteins (Hille et al 1990), one attractive possibility is that secreted tyrosine-sulfated proteins could provide signals that affect development or maintenance of neuronal processes and synaptic function. Secreted proteins, including those in the extracellular matrix (ECM), are known to affect neuronal morphogenesis, synaptic development and function throughout the nervous system (Egles et al 2007;Fox et al 2007;Nishimune et al 2008). Consistent with a potential role for tyrosine-sulfated ECM proteins in regulating synaptic maturation or function is the finding that integrin receptors, which are major mediators of cell-ECM signaling (Hynes 2002), can modulate synaptic development, plasticity and neuronal function in the central nervous system (Chan et al 2006;Cingolani et al 2008;Huang et al 2006;Wakabayashi et al 2008). However, the identities of the key tyrosine-sulfated proteins, their binding partners, and the signaling mechanisms involved in regulating the growth and maintenance of neuronal processes or synaptic maturation and function are currently unknown.

Likewise, the specific tyrosine-sulfated proteins involved in modulating OS structure and morphogenesis, neuronal and synaptic organization, and function in the retina are not yet known. However, laminins are particularly attractive candidates. Laminins are secreted as part of retinal ECM (Hunter et al 1992;Libby et al 2000;Libby et al 1996;Libby et al 1997). Furthermore, deletion of laminin β2 produces deficits with similarities to those in the *Tpst DKO* retina including: disrupted OS formation, impaired retinal function, and ultrastructural aberrations in photoreceptor synapses with apparently normal synapse formation in the IPL (Libby et al 1999). Zebrafish laminin mutants show similar retinal deficits (Biehlmaier et al 2007). Laminins also have important roles in regulating the morphological development and organization of dopaminergic amacrine cells (Denes et al 2007), consistent with the subtle changes noted in the IPL of the *Tpst* DKO retina.

In summary, the current studies demonstrate for the first time that protein-tyrosine sulfation is a significant determinant of proper development and maintenance of retinal function and structure. Furthermore, findings in this report point to a potential role for improper sulfation in human diseases, especially those that affect the nervous system.

Supplementary Material

Refer to Web version on PubMed Central for supplementary material.

Acknowledgments

The project described was partly supported by grants from the National Center For Research Resources (P20RR017703), the National Eye Institute P30EY12190, Oklahoma Center for the Advancement of Science and Technology (OCAST) (DMS), R01 EY007361 (SJF), R01 EY14047 (MEB), R01 HD056022 (KLM), R01 EY14052 and R01 EY018137 (MRA), FFB (MRA), Hope For Vision, NY (MRA), the Reynolds Oklahoma Center on Aging (MRA), and an Unrestricted Grant from Research to Prevent Blindness (SJF). The content is solely the responsibility of the authors and does not necessarily represent the official views of the National Center for Research Resources, the National Eye Institute, or the National Institutes of Health.

We thank Natalia Harmon and Barbara A. Nagel for technical assistance and Drs. Roger Janz and Robert Margolskee for their generous gifts of antisera. The synaptotagmin 2 monoclonal antibody generated by Trevarrow (Trevarrow et al 1990) was obtained from the Zebrafish International Resource Center, which is supported by grant P40 RR012546 from the NIH-NCRR. The Islet-1 monoclonal antibody developed by Ericson (Ericson et al 1992) was obtained from the Developmental Studies Hybridoma Bank developed under the auspices of the NICHD and maintained by the University of Iowa, Department of Biological Sciences, Iowa City, IA 52242.

ABBREVIATIONS

DKO	double knockout
ERG	electroretinography
GCL	ganglion cell layer
GFAP	glial fibrillary acid protein
grt	growth retarded mouse
Hprt	hypoxanthine phosphoribosyltransferase
IHC	immunohistochemistry
ILM	inner limiting membrane
INL	inner nuclear layer
IPL	inner plexiform layer
IPM	interphotoreceptor matrix
IS	inner segment
ONL	outer nuclear layer
OPL	outer plexiform layer
OS	outer segment
P	postnatal day
RHO	rhodopsin
RPE	retinal pigment epithelium
SC	sclera
SDS-PAGE	sodium dodecyl sulfate polyacrylamide gel electrophoresis
TPST	tyrosylprotein sulfotransferase
wt	wild type

REFERENCE LIST

Baylor DA, Lamb TD, Yau KW. Responses of retinal rods to single photons. J.Physiol. 1979; 288:613–634. [PubMed: 112243]

Bettelheim FR. Tyrosine-O-sulfation in a peptide from fibrinogen. J.Amer.Chem.Society. 1954; 76:2838–2839.

Biehlmaier O, Makhankov Y, Neuhauss SC. Impaired retinal differentiation and maintenance in zebrafish laminin mutants. Invest Ophthalmol.Vis.Sci. 2007; 48:2887–2894. [PubMed: 17525225]

Blanks JC, Johnson LV. Selective lectin binding of the developing mouse retina. J.Comp Neurol. 1983; 221:31–41. [PubMed: 6643744]

Blanks JC, Johnson LV. Specific binding of peanut lectin to a class of retinal photoreceptor cells. A species comparison. Invest Ophthalmol.Vis.Sci. 1984; 25:546–557. [PubMed: 6715128]

Borghei A, Ouyang YB, Westmuckett AD, Marcello MR, Landel CP, Evans JP, Moore KL. Targeted disruption of tyrosylprotein sulfotransferase-2, an enzyme that catalyzes post-translational protein tyrosine O-sulfation, causes male infertility. J.Biol.Chem. 2006; 281:9423–9431. [PubMed: 16469738]

Burmeister M, Novak J, Liang MY, Basu S, Ploder L, Hawes NL, Vidgen D, Hoover F, Goldman D, Kalnins VI, Roderick TH, Taylor BA, Hankin MH, McInnes RR. Ocular retardation mouse caused by Chx10 homeobox null allele: impaired retinal progenitor proliferation and bipolar cell differentiation. Nat.Genet. 1996; 12:376–384. [PubMed: 8630490]

Calakos N, Bennett MK, Peterson KE, Scheller RH. Protein-protein interactions contributing to the specificity of intracellular vesicular trafficking. Science. 1994; 263:1146–1149. [PubMed: 8108733]

Chan CS, Weeber EJ, Zong L, Fuchs E, Sweatt JD, Davis RL. Beta 1-integrins are required for hippocampal AMPA receptor-dependent synaptic transmission, synaptic plasticity, and working memory. J.Neurosci. 2006; 26:223–232. [PubMed: 16399691]

Chang YC, Gottlieb DI. Characterization of the proteins purified with monoclonal antibodies to glutamic acid decarboxylase. J.Neurosci. 1988; 8:2123–2130. [PubMed: 3385490]

Cingolani LA, Thalhammer A, Yu LM, Catalano M, Ramos T, Colicos MA, Goda Y. Activity-dependent regulation of synaptic AMPA receptor composition and abundance by beta3 integrins. Neuron. 2008; 58:749–762. [PubMed: 18549786]

Debus E, Weber K, Osborn M. Monoclonal antibodies specific for glial fibrillary acidic (GFA) protein and for each of the neurofilament triplet polypeptides. Differentiation. 1983; 25:193–203. [PubMed: 6198232]

Denes V, Witkovsky P, Koch M, Hunter DD, Pinzon-Duarte G, Brunken WJ. Laminin deficits induce alterations in the development of dopaminergic neurons in the mouse retina. Vis.Neurosci. 2007; 24:549–562. [PubMed: 17711601]

Dowling JE. Synaptic organization of the frog retina: an electron microscopic analysis comparing the retinas of frogs and primates. Proc.R.Soc.Lond B Biol.Sci. 1968; 170:205–228. [PubMed: 4385244]

Egles C, Claudepierre T, Manglapus MK, Champliaud MF, Brunken WJ, Hunter DD. Laminins containing the beta2 chain modulate the precise organization of CNS synapses. Mol.Cell Neurosci. 2007; 34:288–298. [PubMed: 17189701]

Elshatory Y, Deng M, Xie X, Gan L. Expression of the LIM-homeodomain protein Isl1 in the developing and mature mouse retina. J.Comp Neurol. 2007; 503:182–197. [PubMed: 17480014]

Ericson J, Thor S, Edlund T, Jessell TM, Yamada T. Early stages of motor neuron differentiation revealed by expression of homeobox gene Islet-1. Science. 1992; 256:1555–1560. [PubMed: 1350865]

Farjo R, Skaggs J, Quiambao AB, Cooper MJ, Naash MI. Efficient non-viral ocular gene transfer with compacted DNA nanoparticles. PLoS.ONE. 2006; 1:e38. [PubMed: 17183666]

Fox MA, Sanes JR. Synaptotagmin I and II are present in distinct subsets of central synapses. J.Comp Neurol. 2007; 503:280–296. [PubMed: 17492637]

Fox MA, Sanes JR, Borza DB, Eswarakumar VP, Fassler R, Hudson BG, John SW, Ninomiya Y, Pedchenko V, Pfaff SL, Rheault MN, Sado Y, Segal Y, Werle MJ, Umemori H. Distinct target-derived signals organize formation, maturation, and maintenance of motor nerve terminals. Cell. 2007; 129:179–193. [PubMed: 17418794]

Galli T, Zahraoui A, Vaidyanathan VV, Raposo G, Tian JM, Karin M, Niemann H, Louvard D. A novel tetanus neurotoxin-insensitive vesicle-associated membrane protein in SNARE complexes of the apical plasma membrane of epithelial cells. Mol.Biol.cell. 1998; 9:1437–1448. [PubMed: 9614185]

Hille A, Braulke T, von Figura K, Huttner WB. Occurrence of tyrosine sulfate in proteins--a balance sheet. 1. Secretory and lysosomal proteins. Eur.J.Biochem. 1990; 188:577–586. [PubMed: 2331986]

Hille A, Huttner WB. Occurrence of tyrosine sulfate in proteins--a balance sheet. 2. Membrane proteins. Eur.J.Biochem. 1990; 188:587–596. [PubMed: 2331987]

Huang L, Max M, Margolskee RF, Su H, Masland RH, Euler T. G protein subunit G gamma 13 is coexpressed with G alpha o, G beta 3, and G beta 4 in retinal ON bipolar cells. J.Comp Neurol. 2003; 455:1–10. [PubMed: 12454992]

Huang L, Shanker YG, Dubauskaite J, Zheng JZ, Yan W, Rosenzweig S, Spielman AI, Max M, Margolskee RF. Ggamma13 colocalizes with gustducin in taste receptor cells and mediates IP3 responses to bitter denatonium. Nat.Neurosci. 1999; 2:1055–1062. [PubMed: 10570481]

Huang Z, Shimazu K, Woo NH, Zang K, Muller U, Lu B, Reichardt LF. Distinct roles of the beta 1-class integrins at the developing and the mature hippocampal excitatory synapse. J.Neurosci. 2006; 26:11208–11219. [PubMed: 17065460]

Huber G, Matus A. Differences in the cellular distributions of two microtubule-associated proteins, MAP1 and MAP2, in rat brain. J.Neurosci. 1984; 4:151–160. [PubMed: 6198491]

Hunter DD, Murphy MD, Olsson CV, Brunken WJ. S-laminin expression in adult and developing retinae: a potential cue for photoreceptor morphogenesis. Neuron. 1992; 8:399–413. [PubMed: 1550669]

Huttner WB. Sulphation of tyrosine residues-a widespread modification of proteins. Nature. 1982; 299:273–276. [PubMed: 6180325]

Hynes RO. Integrins: bidirectional, allosteric signaling machines. Cell. 2002; 110:673–687. [PubMed: 12297042]

Janz R, Sudhof TC. SV2C is a synaptic vesicle protein with an unusually restricted localization: anatomy of a synaptic vesicle protein family. Neurosci. 1999; 94:1279–1290.

Johnson J, Sherry DM, Liu X, Fremeau RT Jr, Seal RP, Edwards RH, Copenhagen DR. Vesicular glutamate transporter 3 expression identifies glutamatergic amacrine cells in the rodent retina. J.Comp Neurol. 2004; 477:386–398. [PubMed: 15329888]

Kanan Y, Hoffhines A, Rauhauser A, Murray A, Al-Ubaidi MR. Protein tyrosine-O-sulfation in the retina. Exp.Eye Res. 2009; 89:559–567. [PubMed: 19523945]

Kentroti S, Baker R, Lee K, Bruce C, Vernadakis A. Platelet-activating factor increases glutamine synthetase activity in early and late passage C-6 glioma cells. J.Neurosci.Res. 1991; 28:497–506. [PubMed: 1678434]

Krispel CM, Chen CK, Simon MI, Burns ME. Prolonged photoresponses and defective adaptation in rods of Gbeta5−/− mice. J.Neurosci. 2003; 23:6965–6971. [PubMed: 12904457]

Lee RW, Huttner WB. Tyrosine-O-sulfated proteins of PC12 pheochromocytoma cells and their sulfation by a tyrosylprotein sulfotransferase. J.Biol.Chem. 1983; 258:11326–11334. [PubMed: 6577005]

Lem J, Krasnoperova NV, Calvert PD, Kosaras B, Cameron DA, Nicolo M, Makino CL, Sidman RL. Morphological, physiological and biochemical changes in rhodopsin knockout mice. Proc.Natl.Acad.Sci.USA. 1999; 96:736–741. [PubMed: 9892703]

Li X, Mumby SM, Greenwood A, Jope RS. Pertussis toxin-sensitive G protein alpha-subunits: production of monoclonal antibodies and detection of differential increases on differentiation of PC12 and LA-N-5 cells. J.Neurochem. 1995; 64:1107–1117. [PubMed: 7861141]

Libby RT, Champliaud MF, Claudepierre T, Xu Y, Gibbons EP, Koch M, Burgeson RE, Hunter DD, Brunken WJ. Laminin expression in adult and developing retinae: evidence of two novel CNS laminins. J.Neurosci. 2000; 20:6517–6528. [PubMed: 10964957]

Libby RT, Hunter DD, Brunken WJ. Developmental expression of laminin beta 2 in rat retina. Further support for a role in rod morphogenesis. Invest Ophthalmol. Vis. Sci. 1996; 37:1651–1661. [PubMed: 8675409]

Libby RT, Lavallee CR, Balkema GW, Brunken WJ, Hunter DD. Disruption of laminin beta2 chain production causes alterations in morphology and function in the CNS. J.Neurosci. 1999; 19:9399–9411. [PubMed: 10531444]

Libby RT, Xu Y, Selfors LM, Brunken WJ, Hunter DD. Identification of the cellular source of laminin beta2 in adult and developing vertebrate retinae. J.Comp Neurol. 1997; 389:655–667. [PubMed: 9421145]

Moore KL. The biology and enzymology of protein tyrosine O-sulfation. J.Biol.Chem. 2003; 278:24243–24246. [PubMed: 12730193]

Moore KL. Protein tyrosine sulfation: a critical posttranslation modification in plants and animals. Proc.Natl.Acad.Sci.U.S.A. 2009; 106:14741–14742. [PubMed: 19717448]

Nishimune H, Valdez G, Jarad G, Moulson CL, Muller U, Miner JH, Sanes JR. Laminins promote postsynaptic maturation by an autocrine mechanism at the neuromuscular junction. J.cell Biol. 2008; 182:1201–1215. [PubMed: 18794334]

Ouyang Y, Lane WS, Moore KL. Tyrosylprotein sulfotransferase: purification and molecular cloning of an enzyme that catalyzes tyrosine O-sulfation, a common posttranslational modification of eukaryotic proteins. Proc.Natl.Acad.Sci.U.S.A. 1998; 95:2896–2901. [PubMed: 9501187]

Ouyang YB, Crawley JT, Aston CE, Moore KL. Reduced body weight and increased postimplantation fetal death in tyrosylprotein sulfotransferase-1-deficient mice. J.Biol.Chem. 2002; 277:23781–23787. [PubMed: 11964405]

Ouyang YB, Moore KL. Molecular cloning and expression of human and mouse tyrosylprotein sulfotransferase-2 and a tyrosylprotein sulfotransferase homologue in Caenorhabditis elegans. J. Biol. Chem. 1998; 273:24770–24774. [PubMed: 9733778]

Pinazo-Duran MD, Iborra FJ, Pons S, Sevilla-Romero E, Gallego-Pinazo R, Munoz A. Postnatal thyroid hormone supplementation rescues developmental abnormalities induced by congenital-neonatal hypothyroidism in the rat retina. Ophthalmic Res. 2005; 37:225–234. [PubMed: 16006782]

Sameshima M, Uehara F, Ohba N. Specialization of the interphotoreceptor matrices around cone and rod photoreceptor cells in the monkey retina, as revealed by lectin cytochemistry. Exp.Eye Res. 1987; 45:845–863. [PubMed: 3428401]

Sasaki N, Hosoda Y, Nagata A, Ding M, Cheng JM, Miyamoto T, Okano S, Asano A, Miyoshi I, Agui T. A mutation in Tpst2 encoding tyrosylprotein sulfotransferase causes dwarfism associated with hypothyroidism. Mol.Endocrinol. 2007; 21:1713–1721. [PubMed: 17456791]

Sherry DM, Mitchell R, Standifer KM, du Plessis B. Distribution of plasma membrane-associated syntaxins 1 through 4 indicates distinct trafficking functions in the synaptic layers of the mouse retina. BMC.Neurosci. 2006; 7:54. [PubMed: 16839421]

Sherry DM, Wang MM, Bates J, Frishman LJ. Expression of vesicular glutamate transporter 1 in the mouse retina reveals temporal ordering in development of rod vs. cone and ON vs. OFF circuits. J.Comp Neurol. 2003; 465:480–498. [PubMed: 12975811]

Smith TW, Nikulasson S, De Girolami U, De Gennaro LJ. Immunohistochemistry of synapsin I and synaptophysin in human nervous system and neuroendocrine tumors. Applications in diagnostic neuro-oncology. Clin.Neuropathol. 1993; 12:335–342. [PubMed: 8287627]

Stricker HM, Ding XQ, Quiambao A, Fliesler SJ, Naash MI. The C214S mutation in peripherin/rds causes a loss-of-function phenotype in transgenic mice. Biochem.J. 2005; 388:605–613. [PubMed: 15656787]

Tan E, Wang Q, Quiambao AB, Xu X, Qtaishat NM, Peachey NS, Lem J, Fliesler SJ, Pepperberg DR, Naash MI, Al Ubaidi MR. The relationship between opsin overexpression and photoreceptor degeneration. Invest Ophthalmol.Vis.Sci. 2001; 42:589–600. [PubMed: 11222515]

Trevarrow B, Marks DL, Kimmel CB. Organization of hindbrain segments in the zebrafish embryo. Neuron. 1990; 4:669–679. [PubMed: 2344406]

Wakabayashi Y, Tsujimura A, Matsuda K, Yoshimura N, Kawata M. Appearance of LFA-1 in the initial stage of synaptogenesis of developing hippocampal neurons. Arch.Histol.Cytol. 2008; 71:23–36. [PubMed: 18622091]

Wässle H, Puller C, Muller F, Haverkamp S. Cone contacts, mosaics, and territories of bipolar cells in the mouse retina. J.Neurosci. 2009; 29:106–117. [PubMed: 19129389]

Westmuckett AD, Hoffhines AJ, Borghei A, Moore KL. Early postnatal pulmonary failure and primary hypothyroidism in mice with combined TPST-1 and TPST-2 deficiency. Gen.Comp Endocrinol. 2008; 156:145–153. [PubMed: 18243191]

Xu X, Quiambao AB, Roveri L, Pardue MT, Marx JL, Röhlich P, Peachey NS, Al-Ubaidi MR. Degeneration of cone photoreceptors induced by expression of the *Mas1* proto-oncogene. Exp.Neurol. 2000; 163:207–219. [PubMed: 10785460]

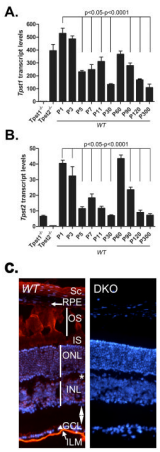

Figure 1. Postnatal developmental steady-state levels of *Tpst1* and *Tpst2* transcripts in the mouse retina

Relative quantitative real time RT-PCR (qRT-PCR) for *Tpst1* (A) and *Tpst2* (B) was performed and each presented value was determined from two independent analyses each performed in triplicate on 3–5 individual samples. Data were plotted using Prism (GraphPad Software). Error bars represent S.E.M. Both $Tpst1^{-/-}$ and $Tpst2^{-/-}$ retinas were obtained from mice at postnatal (P) day 30.*WT*; wild type. (C), immunohistochemical localization of tyrosine-sulfated proteins. Wild-type (*WT*) and $Tpst1^{-/-}$ and $Tpst2^{-/-}$ double knockout (DKO) retinas were probed with the PSG2 antibody. Labeling of the *WT* retina is found in sclera (Sc), retinal pigment epithelium (RPE), photoreceptor outer segments (OS), inner segments (IS), outer nuclear layer (ONL), outer plexiform layer (OPL), inner nuclear layer (INL), inner plexiform layer (IPL) and ganglion cell layer (GCL). Asterisk between ONL and INL is marking the OPL and double-headed arrow between INL and GCL denotes IPL. Red, PSG2; blue, DAPI.

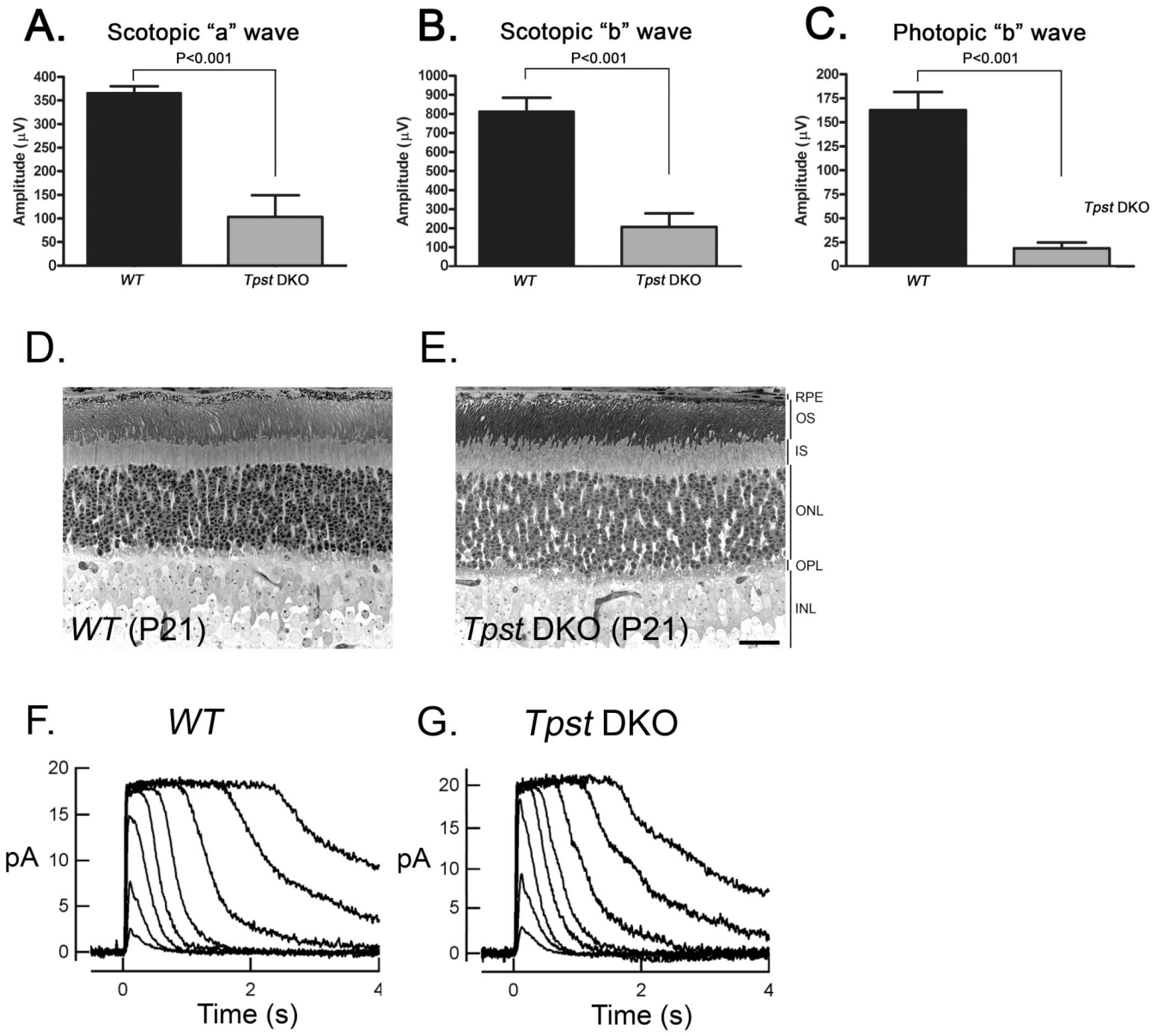

Figure 2. Functional and structural evaluation of normal and *Tpst* DKO retinas

A, scotopic rod responses to 17.5dB flashes in the dark represented by the *a*-wave. **B,** scotopic *b*-wave responses to 17.5dB flashes representing responses from bipolar and possibly other neurons in the retina. **C**, photopic cone responses to 15dB light flashes under adapting light represented by the photopic *b*-wave. Statistical significance is indicated above the bar graphs. Error bars represent S.E.M. (n=3 for *Tpst* DKO and 8 for *wt*). Histologic analysis of retinas from wild-type (*wt*; D) and $Tpst1^{-/-}$ and $Tpst2^{-/-}$ double knockout (*Tpst* DKO; E). Scale Bar in E represents 50 μm. **E&F**, flash response families from rods in normal and *Tpst* DKO retinas. Flash strengths (in photons μm^{-2}) varied from roughly 16–92,000 by factors of 4 for DKO rods. A, recordings from *wt*; B, recordings from *Tpst* DKO.

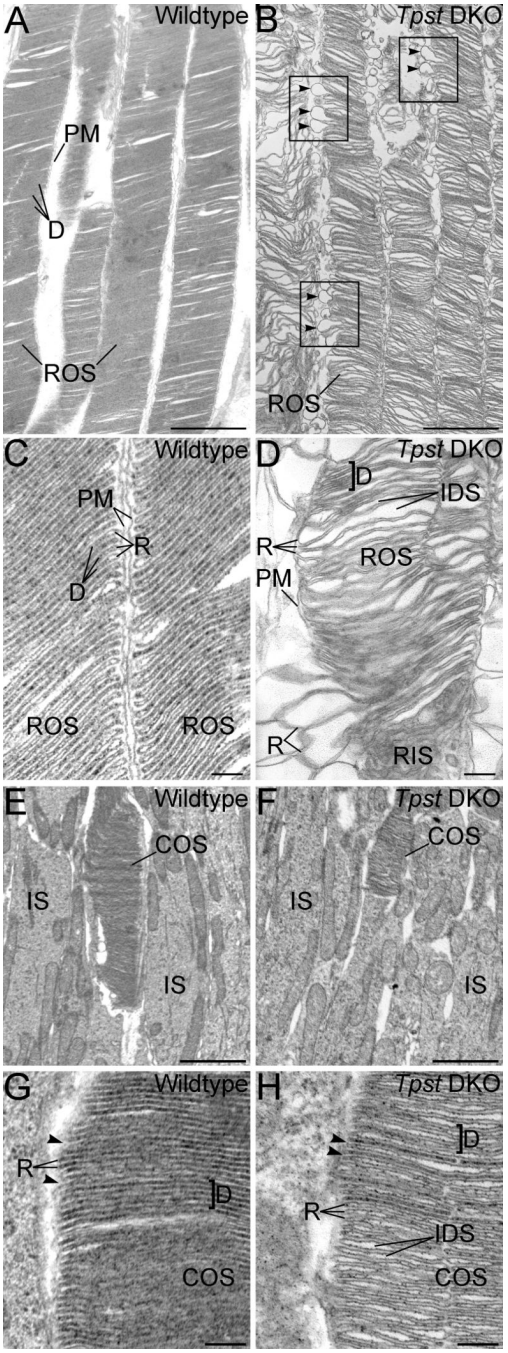

Figure 3. Outer segment ultrastructure in normal and *Tpst* DKO retinas

A–B: Electron microscopy of rod outer segments (ROS) in wild-type (*wt*; **A**) and *Tpst1*$^{-/-}$ and *Tpst2*$^{-/-}$ double knockout (*Tpst* DKO; **B**) retinas. ROSs in the *wt* retina has normal organization with tightly stacked discs (D) surrounded by the plasma membrane (PM). ROS organization is severely disrupted in the *Tpst* DKO. Large swirls of membrane are present in the space between outer segments. Discs are irregular in size and shape and often appear to protrude into the extracellular space (boxes and arrowheads). **C–D:** ROS ultrastructure at higher magnification in *wt* (**C**) and *Tpst* DKO (**D**) retinas. ROS in the *wt* retina (**C**) has normal ultrastructure with tightly packed, flattened discs (D) and the typical hairpin appearance of the disc rim (R). The discs are separate from the surrounding plasma

membrane (PM) and show very little intradiscal space. In the *Tpst* DKO retina, the ultrastructural organization of the discs and the plasma membrane of ROSs are severely disrupted (**D**). The intradiscal space (IDS) is greatly enlarged and the hairpin structure of the disc rim is often disrupted. Whorls of ROS membrane are present between ROSs, often appearing to protrude from abnormal ROS discs. The inner segment of the cell is also visible (RIS). E–F: Cone outer segment (COS) ultrastructure in *wt* (E) and *Tpst* DKO (F) retinas. COSs in the *wt* retina (E) show normal ultrastructure with tightly packed, flattened discs (D) and typical appearance of the disc rim (R). The interdiscal space is continuous with the extracellular space (arrowheads). The discs show very little intradiscal space. In the *Tpst* DKO retina (F), the ultrastructural organization of the discs in the COS is largely normal, although the intradiscal space (IDS) is somewhat enlarged in some discs. G–H: COS ultrastructure at higher magnification in *wt* (G) and *Tpst* DKO (H) retinas. In *wt* retina (G), COS discs (D) show normal rim structure, flattened morphology and tightly stacked arrangement. The space between disks is continuous with the extracellular space (arrowheads). In the *Tpst* DKO retina (H), COS discs are tightly packed and have a flattened structure, but the intradiscal space (IDS) is often slightly enlarged compared to *wt*. Rim structure is relatively normal. The space between disks is continuous with the extracellular space (arrowheads). Scale bars represent 2 μm for A–B, E–F; 250 nm for C–D; 500 nm for G–H.

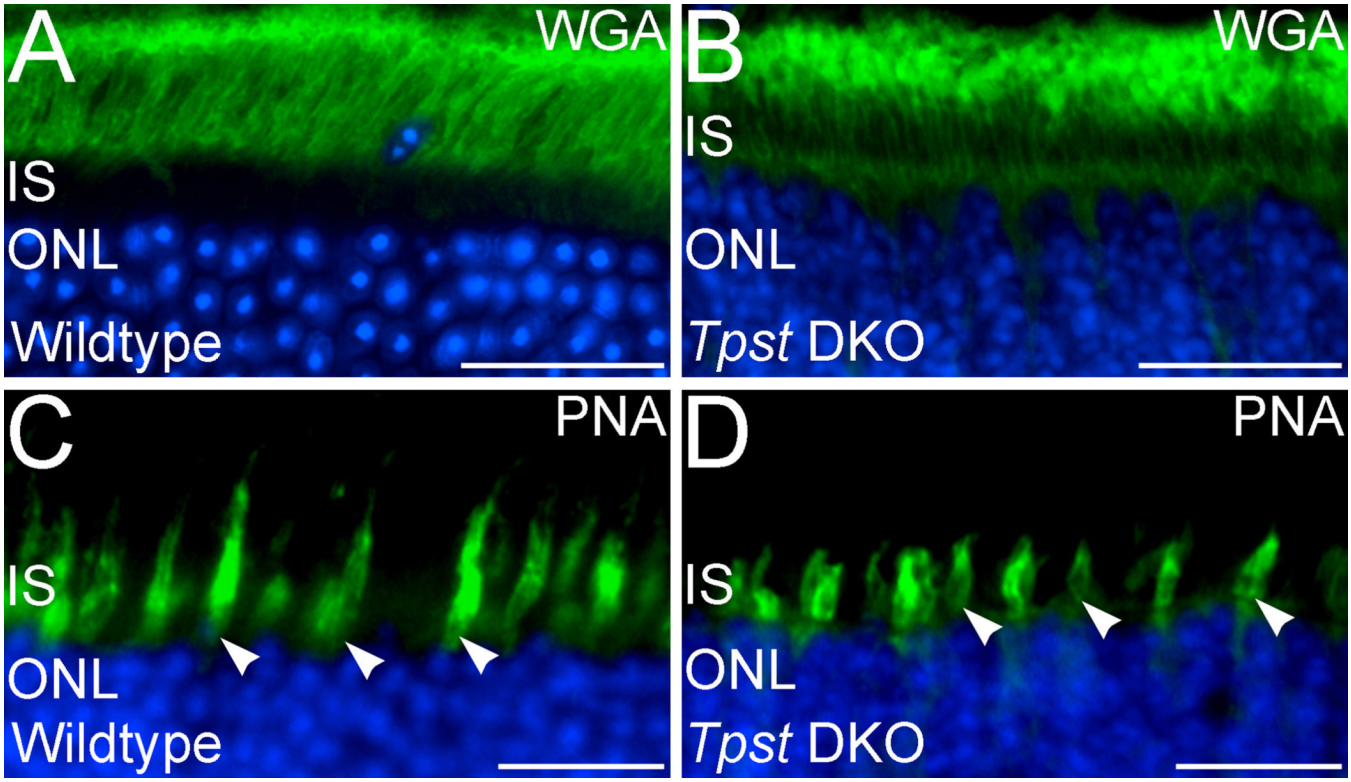

Figure 4. Rod and cone interphotoreceptor matrix (IPM) in *wt* and *Tpst* DKO retinas

A–B: In the *wt* retina (A), the IPM associated with ROS is labeled by WGA (green). In the *Tpst* DKO retina (B), the IPM associated with ROS also is labeled by WGA, although ROS organization is not as well preserved as in *wt* retina. C–D: In the *wt* retina (C), the IPM associated with cones is labeled by PNA (green, arrowheads). In the *Tpst* DKO retina (D), the IPM associated with cones is also present and labeled by PNA (arrowheads), although the sheath around the cone OS is reduced compared to *wt* retina. Photoreceptor nuclei in the outer nuclear layer (ONL) are counterstained with DAPI (blue) in all panels. IS, inner segments. Scale bars represent 20 μm for all panels.

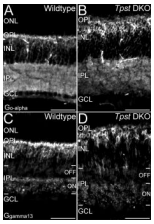

Figure 5. Expression of G-protein subunits associated with transmission to ON bipolar cells is retained in the *Tpst* DKO retina

A–B: $G_{\alpha o}$ is present in all ON-cone and rod bipolar cells and their dendrites in the outer plexiform layer (OPL) in the *wt* retina (**A**). $G_{\alpha o}$ labeling is retained in the ON-cone and rod bipolar cells of the *Tpst* DKO retina (**B**). **C–D:** Labeling for Gγ13 is present in the dendrites, cell bodies and terminals of ON-cone and rod bipolar cells in the *wt* retina (**C**). Gγ13 labeling is retained in ON-cone and rod bipolar cells in the *Tpst* DKO retina (**D**). Note that ON-cone and rod bipolar cell terminals stratify properly in the ON sublamina of the inner plexiform layer (IPL) in the *Tpst* DKO retina. Labeling of blood vessels (bv) in **A** and **B** is non-specific. ONL, outer nuclear layer; GCL, ganglion cell layer. Scale bars represent 50 μm for all panels.

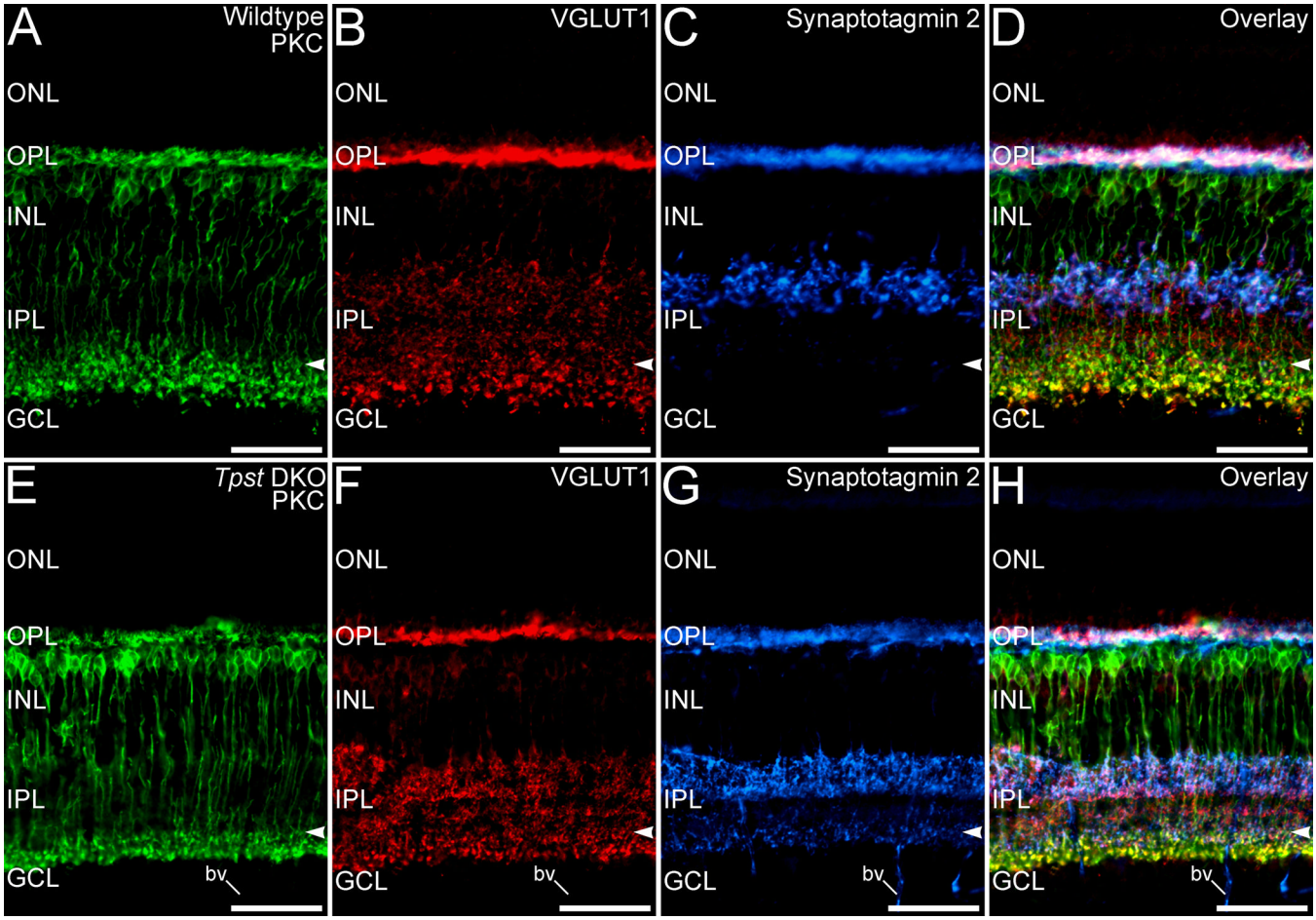

Figure 6. Laminar organization of the inner plexiform layer (IPL) is retained in the *Tpst* DKO retina

A–D: Normal laminar organization of the bipolar cell terminals in the IPL in *wt* retina. Protein kinase C (PKC, *green*) labels rod bipolar cells and their large terminals in the innermost inner plexiform layer (IPL). Vesicular glutamate transporter 1 (VGLUT1, *red*) is expressed in all bipolar cell terminals throughout the IPL. Synaptotagmin 2 (blue) labels Type 2 OFF-cone bipolar cells that terminate in the outer portion of the IPL and Type 6 ON-cone bipolar cells and their sparse terminal plexus in the inner portion of the IPL (*arrowhead*). E–H: The laminar organization of the IPL remains intact in the *Tpst1*$^{-/-}$ and *Tpst2*$^{-/-}$ double knockout (*Tpst* DKO) retina. Rod bipolar cells project properly to the innermost portion of the IPL and VGLUT1 labeling is present in bipolar cell terminals at all levels of the IPL, as appropriate. The terminals of the Type 2 OFF-cone bipolar cells and Type 6 ON-cone bipolar cells also project properly to the OFF and ON sublayers of the IPL, respectively, although the Type 6 ON-cone bipolar cell plexus in the ON sublamina of the IPL is expanded in the *Tpst* DKO retina (arrowheads). Labeling of blood vessels (bv) is non-specific. ONL, outer nuclear layer; OPL, outer plexiform layer; INL, inner nuclear layer; IPL, inner plexiform layer; GCL, ganglion cell layer. Scale bars represent 50 μm.

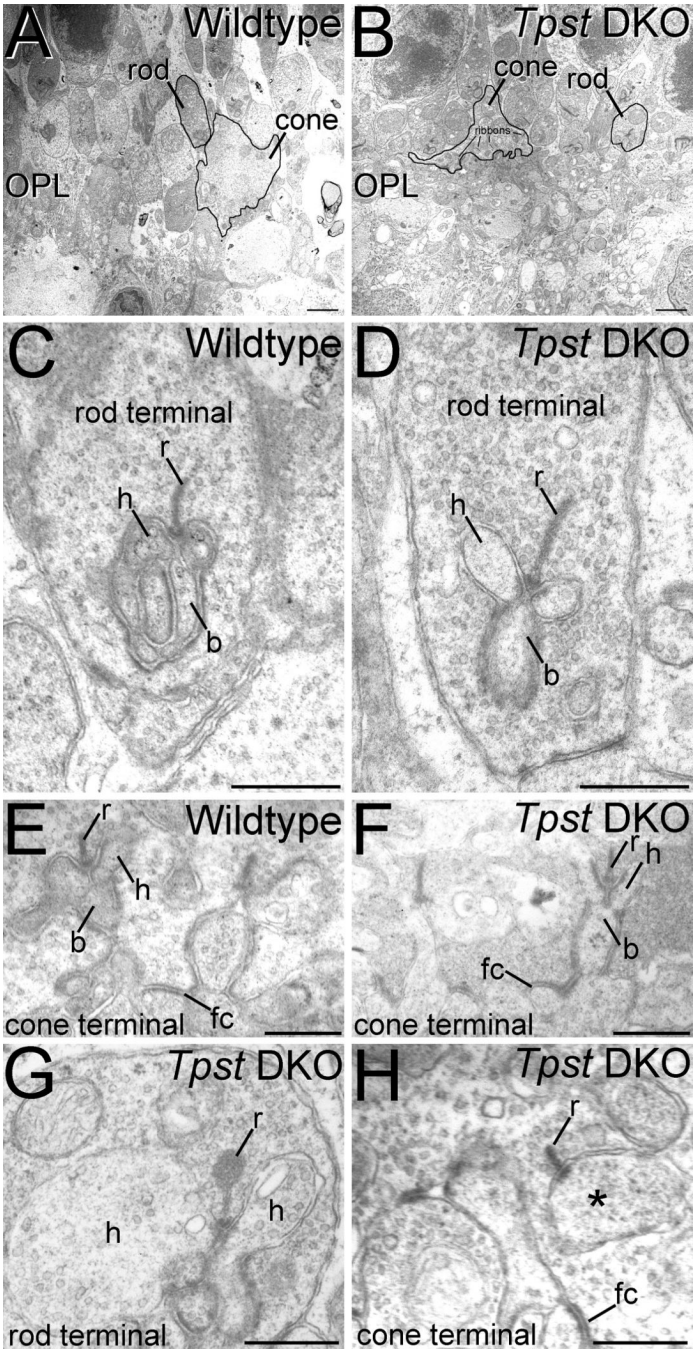

Figure 7. Lack of tyrosine sulfation degrades outer plexiform layer (OPL) structure, but synapse formation by photoreceptors still occurs

A–B: Low magnification electron micrographs of the OPL in wild-type *wt* (**A**) and *Tpst1*$^{-/-}$ and *Tpst2*$^{-/-}$ double knockout (*Tpst* DKO) (**B**) retinas show the normal structure of the OPL, with the photoreceptor terminals located distally and the processes of second-order neurons located proximally. However, the photoreceptor terminals in the OPL of the *Tpst* DKO retina showed irregular spacing and often showed ultrastructural abnormalities, such as ectopic synaptic ribbons or ribbons that were not anchored to the presynaptic membrane of the terminal (see ribbons in the cone terminal), even though terminals with normal synapses were also present. C–D: Rods in the *wt* (C) and *Tpst* DKO (D) retina formed

normal ribbon synaptic complexes with synaptic ribbons (r) and synaptic vesicles presynaptically, and appropriately oriented horizontal cell processes (h) and bipolar cell processes (b) postsynaptically. E–F: Cones in the *wt* (E) and *Tpst* DKO (F) also formed normal ribbon synaptic complexes. Flat contacts (fc) between cones and OFF-cone bipolar cells also show normal ultrastructure in the absence of TPST-1 and TPST-2. G and H: Although photoreceptors did form normal synapses in the *Tpst* DKO retina, a variety of ultrastructural aberrations were observed in synapses made by rod (G) and cone (H) terminals in the absence of protein sulfation. Scale bars represent 2 μm for A–B; 0.5 μm for C–H.

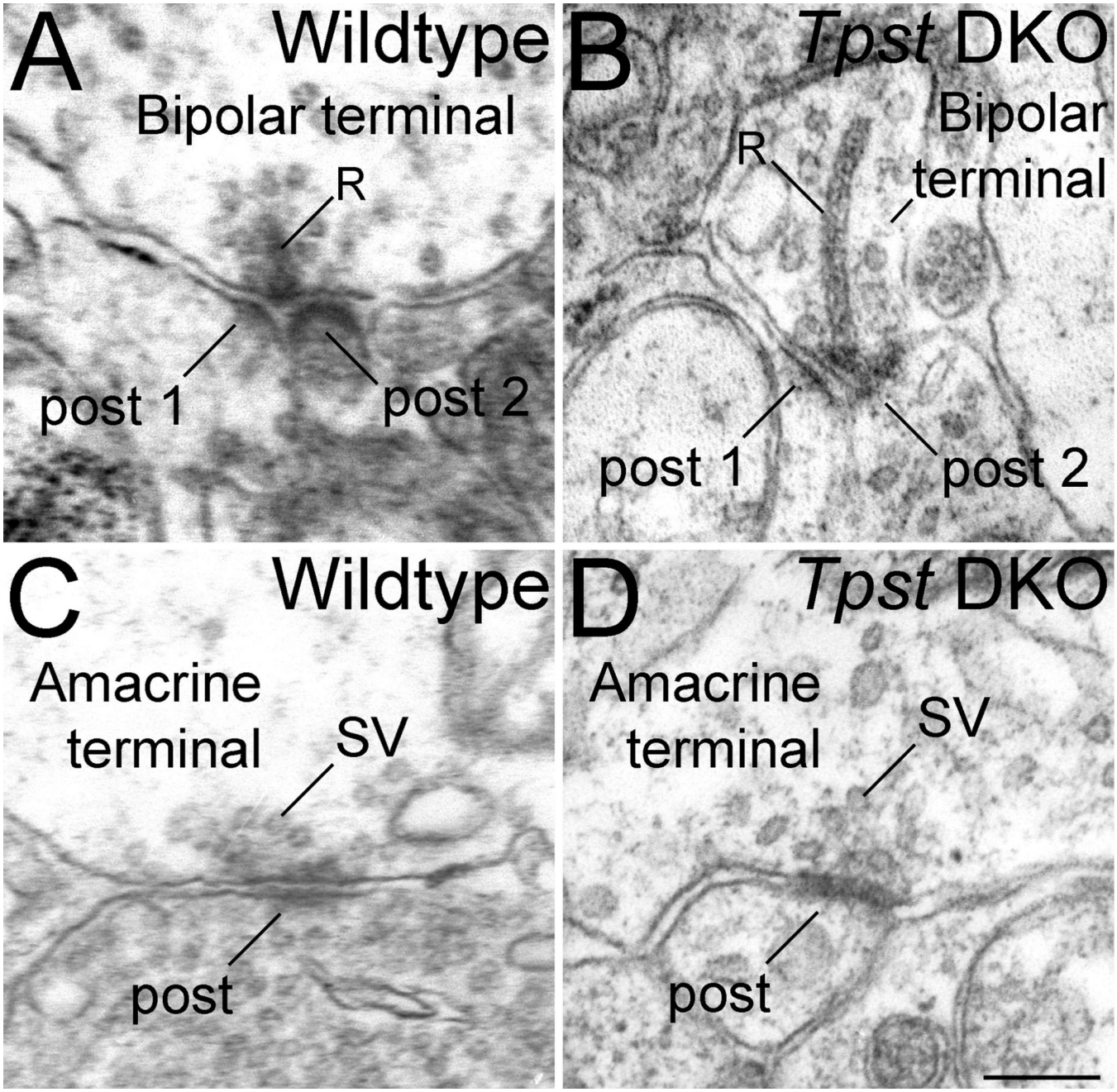

Figure 8. Tyrosine sulfation is not essential for synapse formation by bipolar cells and amacrine cells in the inner plexiform layer

A–B: Bipolar cell ribbon synapses show normal diad ultrastructure in retinas from *wt* (*wt*) (**A**) and *Tpst1*$^{-/-}$ and *Tpst2*$^{-/-}$ double knockout (*Tpst* DKO; **B**) mice. Bipolar cell synapses are organized around a synaptic ribbon (R) with a halo of synaptic vesicles in the presynaptic bipolar cell terminal. Two post-synaptic processes (post-1 and -2) arising from amacrine or ganglion cells flank the ribbon and show the typical densification of the post-synaptic membrane. **C–D:** Conventional synapses made by amacrine cells have normal ultrastructure in the *wt* (**C**) and *Tpst* DKO retina (**D**). The presynaptic terminal of conventional synapses have the usual clustering of synaptic vesicles (SV) at the active zone,

a synaptic cleft, and a post-synaptic density in the post-synaptic process (post). Scale bar represents 0.2 μm for all panels.

Table 1

Characteristics of dark-adapted mouse rods.

	Dark current (pA)	Time to peak (ms)	τ_{rec} (ms)	Integration time (ms)	Elementary amplitude (pA)	I_o† (photons/μm^2)	τ_D (ms)
WT	15.4 ± 0.7 (28)	113 ± 3 (28)	199 ± 14 (27)	264 ± 14 (27)	0.57 ± 0.04 (27)	52.1 ± 2.7 (28)	250 ± 9 (28)
Tpst* DKO	10.1 ± 2.1 (7)	122 ± 9 (7)	166 ± 26 (7)	285 ± 25 (7)	0.50 ± 0.11 (7)	72.2 ± 12.5 (7)	159 ± 6 (7)

The 'elementary amplitude', also referred to as the single photon response, is the response generated by a single photon absorption.

† Flash strength that elicited a half-maximal response.

* No cells were discarded; data includes cells with small dark currents (range 5.4 – 20.6 pA). No rods drawn into the suction electrode were unresponsive.

Values represent mean ± s.e.m.

The number of rods used to determine each parameter presented is given in parentheses.

τ_{rec} is the time constant of recovery for dim flashes, and τ_D is the dominant time constant of recovery measured from saturating flashes.